Chapter 5

Clusters Associated with Ae/Be Stars

In this Chapter we use our infrared images to investigate the stellar environments of Ae/Be stars on local scales (over fields $<<$ 1 pc in diameter). We are particularly interested in the clustering properties in these isolated star formation sites. Our first task is to quantify our definition of "a cluster" which, as already stated, can not be done from either our molecular column density maps or our optical source count radial profiles. Next, in order to make comparisons between different isolated star-forming sites containing Ae/Be stars, we scale our heterogeneous set of infrared images to the same physical area in pc^2 for each region, and determine stellar census counts. We then revisit the issue of survey sensitivity (first presented in Chapter 3) and discuss the possibility of contamination by foreground / background stars. After satisfying ourselves that we have accounted for these effects to the best of our ability given the available data, we then examine a correlation of local stellar surface density with Ae/Be mass, and present one physical interpretation of this correlation. Finally, we compare our results on stellar surface densities near Ae/Be stars, to other similarly young star forming regions as well as to older regions containing similarly isolated high-mass stars.

5.1 Definition of Size Scale for Investigation of Clustering Properties

Because of the peculiar morphological structure of the molecular gas distributions (apparently disturbed clouds which are not centered on the Ae/Be stars themselves), we can not use information on cloud sizes to fix the size scale

over which we should investigate the stellar clustering properties. Furthermore, because at least half of the aggregate members appear to be embedded sources, we can not use radial density profiles constructed from our large-field optical frames to investigate the clustering properties, or even to fix the typical cluster radii. Finally, because the infrared frames are small in angular size, in the typical case we cannot use them to construct radial density profiles and look for central enhancements.

Therefore, to determine an appropriate size scale over which to investigate source clustering in the vicinity of Ae/Be stars, we examine one case in which the boundaries of the optical and infrared clusters are clearly delineated, and which we feel justified in using as a template with which to investigate other Ae/Be regions. The BD +40° 4124 environment is shown in Figure 5.1; in the left panel is a large-scale field centered on the Ae/Be star at R-band, and in the right panel an expanded field at K-band. The small stellar aggregate clearly seen in the infrared image is isolated by about 0.7 pc from the Hα -emission rim seen in the optical image (which bounds the molecular gas distribution, as seen in Figure 2.1). Important to our arguments on the definition of "a cluster," is that the region between the aggregate and the bright-rim / edge-of-cloud appears to be relatively devoid of optical or infrared sources. Of the 33 stars detected to a 10σ limit on this K-band image, 26, or 79%, are contained within the central 1.4 arcmin^2 while only 21% are found in the outer 3.6 arcmin^2 of the frame. Because the number of sources in this region is high (at least higher than the average for the central Ae/Be aggregates; see below), we are able to quantify the visual impression of clustering with radial surface and volume density plots, which indeed demonstrate this group to represent a stellar density enhancement approximately 0.15pc in projected radius.

Figure 5.1. *The star-forming environment of the Ae/Be star BD +40° 4124.* We show, in the left panel, a 23 arcmin × 23 arcmin field centered on the Ae/Be star at R-band, and, in the right panel, an expanded field at K-band. We use this region as a template for defining the fiducial size scale over which to investigate stellar clustering properties near Ae/Be stars. Based on stellar radial density plots constructed from these images, we choose a size scale of 1/3 pc × 1/3 pc for this purpose.

BD+40° 4124 REGION

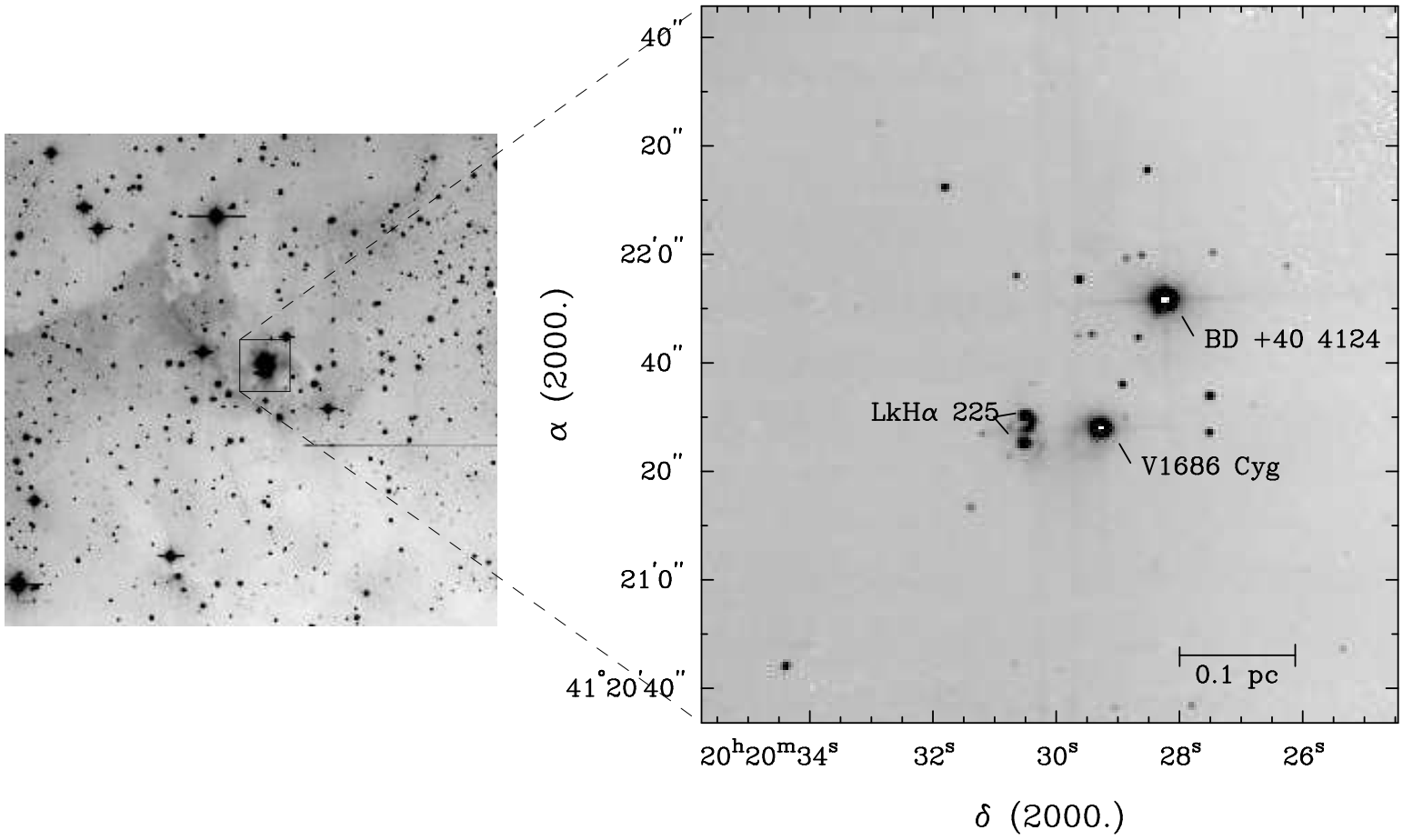

Unfortunately, due to the sometimes small number of sources found in association with Ae/Be stars, we are unable to make radial density profiles with meaningful bin sizes for every region. However, with evidence that the BD +40° 4124 group is a relatively isolated cluster of stars identified by the presence of an Ae/Be star, we have chosen to investigate the other members of our sample over an area in pc^2 equivalent to that subtended by the BD +40° 4124 cluster. We perform this exercise at K-band in the next section. We note the dynamical significance of the chosen scale ($1/3 \times 1/3$ pc or approximately 0.167 pc in radius) is that it translates into a crossing time of about 0.3 Myr for a canonical velocity dispersion of 1 km s^{-1} (Benson & Myers 1989 and Loren 1989 for molecular gas; Jones & Walker 1988 for stars in an expanding cluster). This timescale is comparable to the inferred ages for the Ae/Be stars themselves and thus ensures us of capturing in our survey, any stars born nearly coevally with the central Ae/Be star.

5.2 K-band Images and Source Counts

In Figure 5.2 we present K-band images centered on the young, isolated Ae/Be stars in our sample, covering 1/3 pc in each dimension. These images are organized in order of decreasing Ae/Be mass (from 26 to 3 $M_\odot$), and demonstrate the presence of (in most cases) previously unknown, lower-mass companions within 0.167 pc of all Ae/Be stars surveyed in this program. Comparison of the BD +40° 4124 panel in Figure 5.2 with the larger field infrared image in Figure 5.1, shows that our chosen size scale seems appropriate for addressing the issue of clustering in the BD +40° 4124 region. We extrapolate that it is also appropriate in the other isolated star-forming environments containing young high-mass stars. The remainder of this Chapter consists of an analysis of Ae/Be clustering properties based on these infrared images.

Figure 5.2. *K-band images uniformly covering 1/3pc × 1/3pc for 17 Ae/Be regions.* The images are centered on the Ae/Be star itself and were obtained with the University of Massachusetts NICMASS camera mounted on the MDM 2.4m and 1.3m telescopes, and with the Kitt Peak National Observatory SQIID camera mounted on the KPNO 50in telescope; the range of platescales is from 0.4-1.3 arcsec pixel^{-1}. The range in resolution combined with the range in source distance causes the apparent differences in signal - to - noise between our infrared images when they are scaled to the same physical area in square pc, as we have done here. The images are organized in order of decreasing Ae/Be mass (from top to bottom and left to right), and range from 26 $M_{\odot}$ down to 3 $M_{\odot}$. These data constitute our entire infrared survey sample except for those Ae/Be stars located near the Orion, NGC 2264, or Taurus star-forming complexes.

MWC297 (NICMASS / MDM 2.4m)

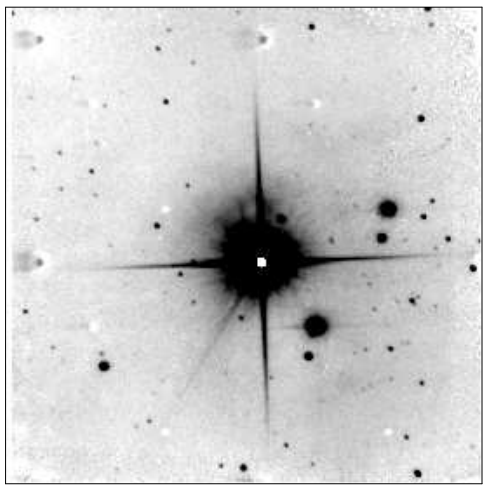

δ

α

BD+40 4124 (NICMASS / MDM 2.4m)

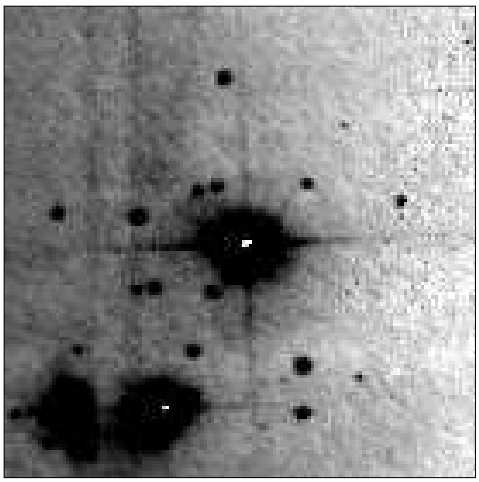

δ

α

MWC1080 (NICMASS / MDM 2.4m)

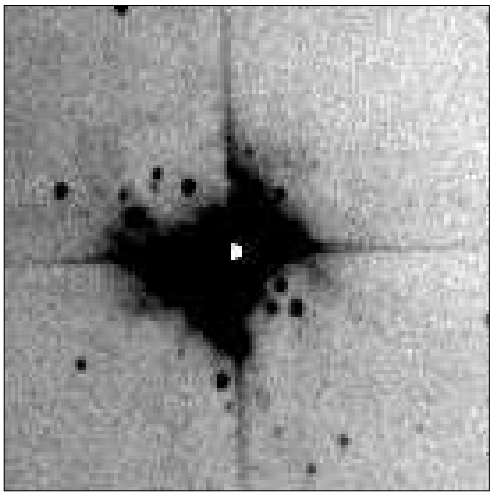

δ

α

LkHa198/V376Cas (NICMASS / MDM 1.3m)

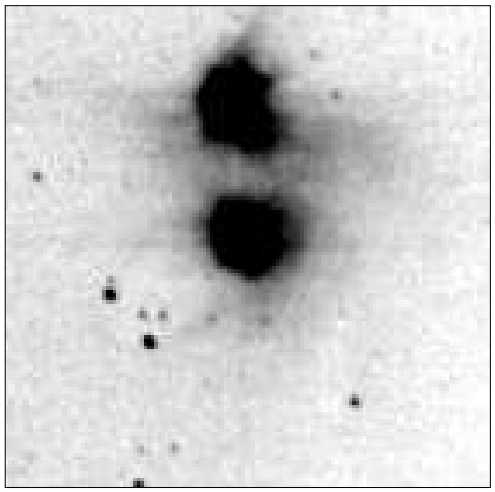

δ

α

MWC137 (NICMASS / MDM 1.3m)

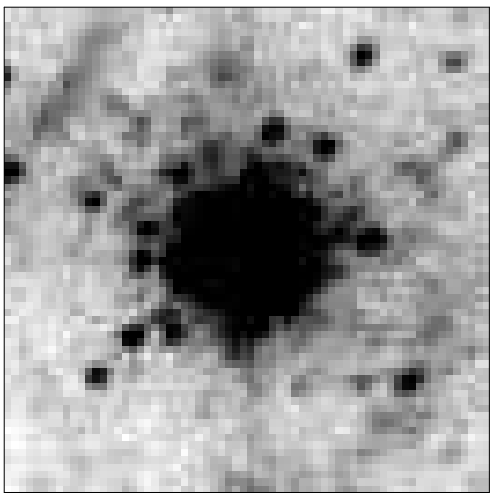

δ

α

LkHa215 (NICMASS / MDM 2.4m)

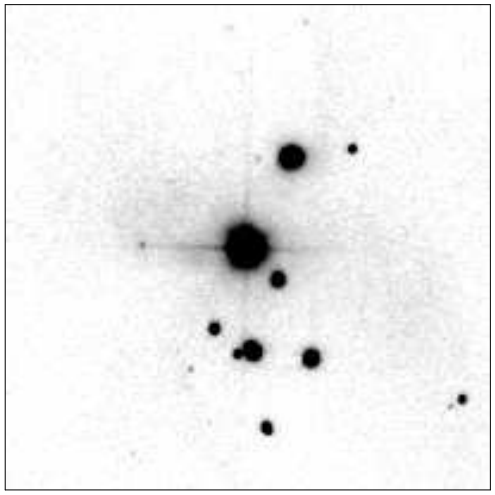

δ

α

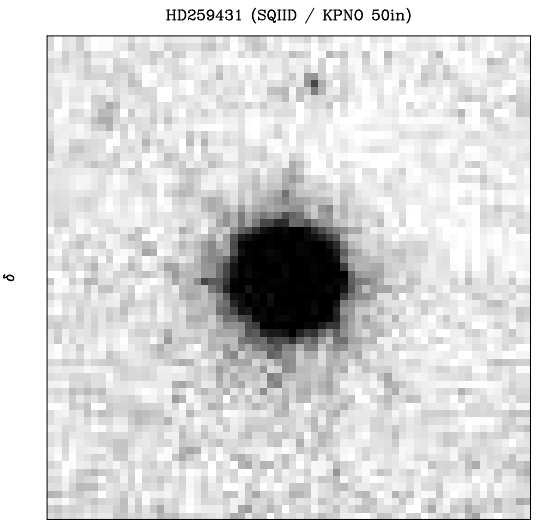
HD259431 (SQIID / KPNO 50in)
δ
α

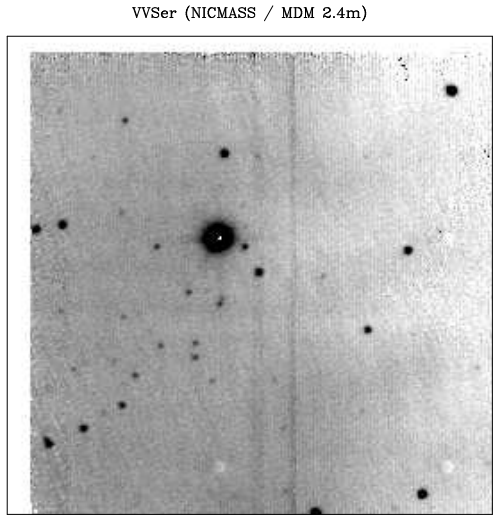
VVSer (NICMASS / MDM 2.4m)
δ
α

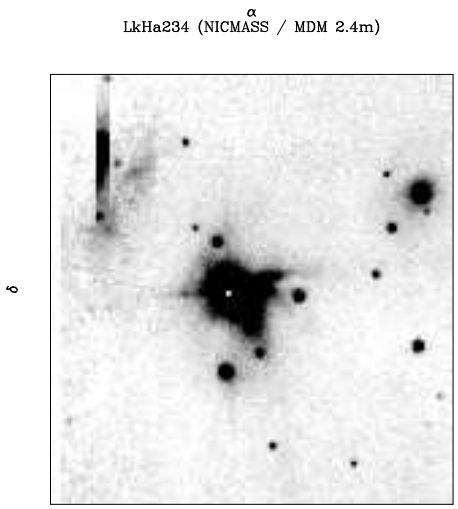
LkHa234 (NICMASS / MDM 2.4m)
δ
α

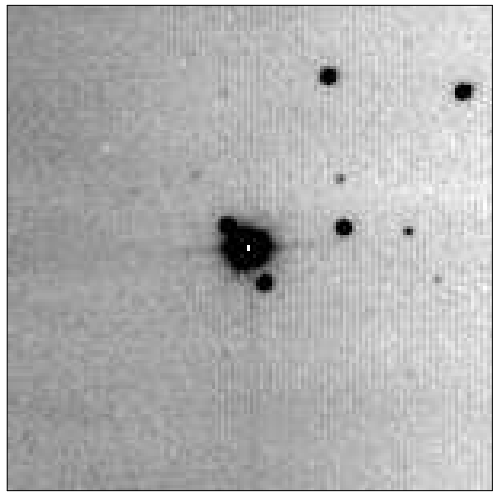
BD+46 3471 (NICMASS / MDM 2.4m)
δ
α

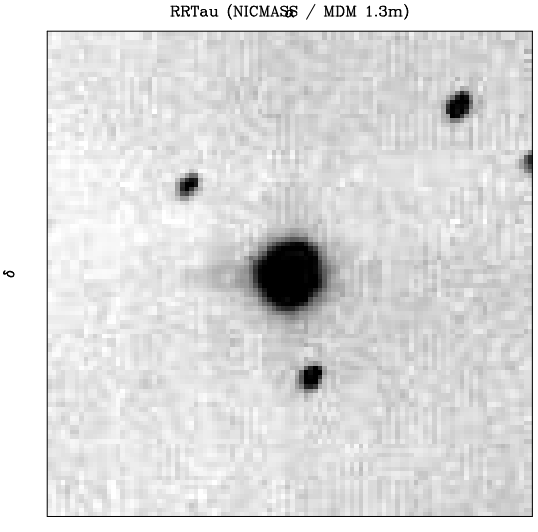
RRTau (NICMASS / MDM 1.3m)
δ
α

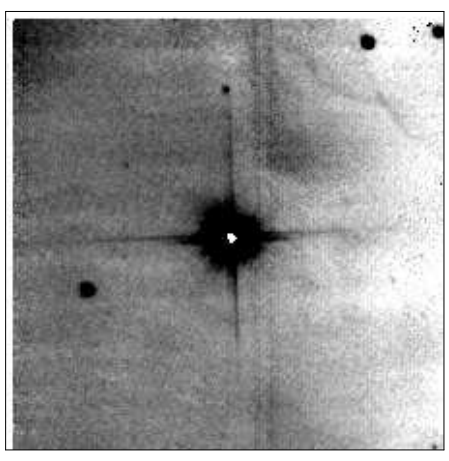
HD200775 (NICMASS / MDM 2.4m)
δ
α

BD+61 154 (NICMASS / MDM 2.4m)

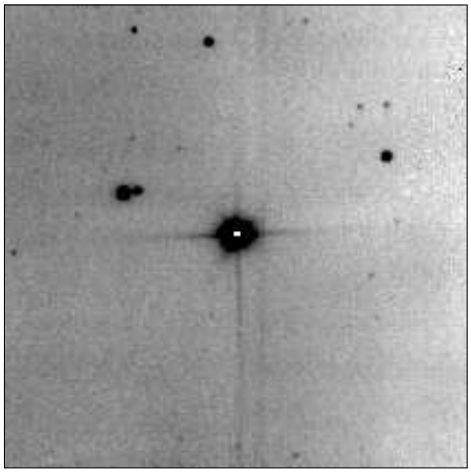

δ

α

LkHa 208 (NICMASS / MDM 1.3m)

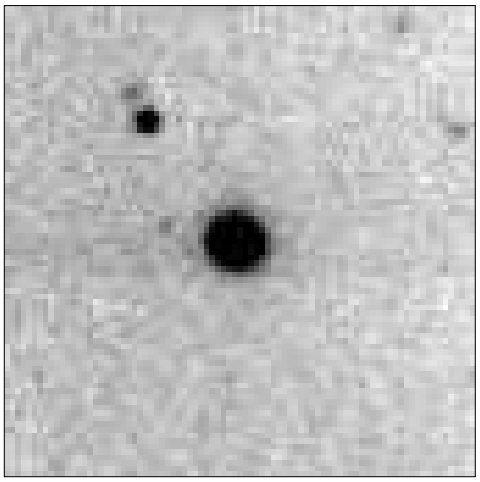

δ

α

HD250550 (NICMASS / MDM 1.3m)

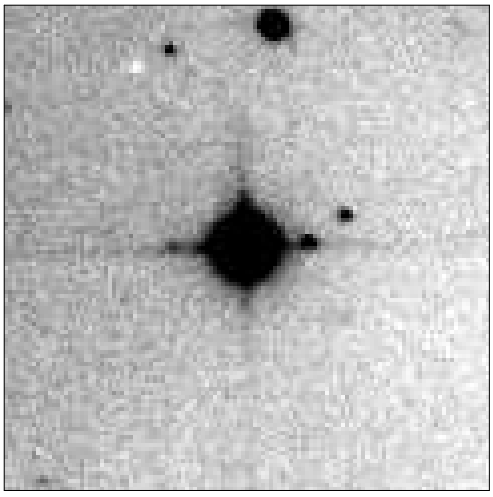

δ

α

LkHa 218 (NICMASS / MDM 1.3m)

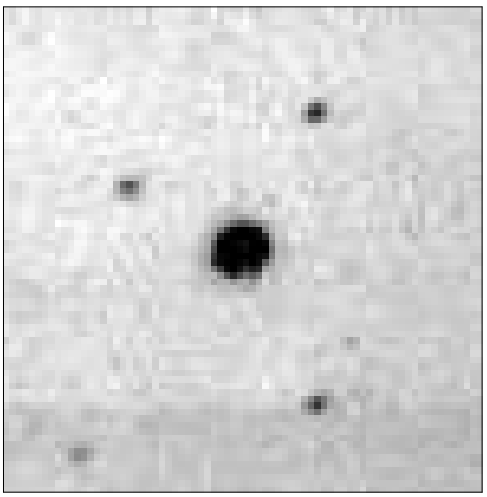

δ

α

LkHa233 (SQIID / KPNO 50in)

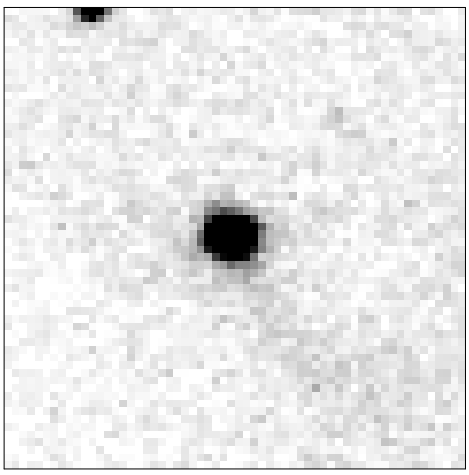

δ

α

Our particular focus is on addressing the issue of stellar surface densities. We must thus extract from our images, the number of stars found within the 1/3 pc $\times$ 1/3 pc sub-image of each Ae/Be region displayed in Figure 5.2. The nature of the infrared companions to the Ae/Be stars will be discussed in subsquent Chapters. At the present time, we anticipate our findings in those Chapters and assert, based on 1) infrared excesses and optical emission line features indicative of stellar youth (Chapter 6) and 2) actual location on pre-main sequence isochrones of < 3 Myr (Chapter 8), that the majority of the members of these small clusters must also be young stars. We also remind the reader of our notation from the optical images that many of the nearby companions to the Ae/Be stars have the appearance of so-called "socket stars." We thus proceed under the assumption that all stars seen projected within 0.167 pc of the Ae/Be stars are indeed physically associated with the molecular core.

Our summary on clustering properties within the Ae/Be subimages can be found in Table 5.1, also organized in order of decreasing Ae/Be mass. We give the number companions detected on our infrared images over 1/3 pc $\times$ 1/3 pc size scales in Column (5). In Column (6) we give entries for the number of these infrared companions with optical counterparts. Depending on the region, between 25% and 100% of the infrared cluster members are also optically detected. In Columns (7) and (8) we quote the numbers of spectra obtained over the inner 0.167 pc areas and a summary of approximate spectral types. We note that in most regions additional spectroscopic data do exist over the greater extent of the cloud.

How uniform is our infrared survey data? Due to the combined effects of 1) instrumental heterogeneity of the infrared data itself and 2) variations in source distances, our initial infrared source counts are not to a strictly uniform sensitivity level to stellar populations of varying mass, age, and line-of-sight extinction between Ae/Be regions. As we will show, however, the sensitivity corrections

Table 5.1. Summary of Cluster Parameters at $r < 0.167$ pc

Name	Mass $M_\odot$	Relative Distance	Rel. Inst. Sensitivity	IR Stars Detected	Opt. Stars Detected	# with Spectra	Comment on Spectra
(1)	(2)	(3)	(4)	(5)	(6)	(7)	(8)
MWC 297	26.5	0.45	1.0	41	9	4	1 Be, 2 GK, 1 cont+e star
MWC 1080	20.6	1.00	0.5	30	8	5	1 Be, 1 K, 2 Me, 1 M
MWC 137	18.9	1.30	0.7	26	12	9	1 Be, 1 F, 5 GK(e?), 2 M(e?)
BD +40° 4124	12.6	1.00	1.0	22	10	10	2 Be, 2 AFe, 1F, 2 Ke, 3Me
Lk Hα 198	9.6	0.60	0.4	19	14	2	2 Ae
Lk Hα 215	9.5	0.80	1.0	15	11	11	1 Be, 8 Me , 2 M
HD 259431	8.9	0.80	>0.3	3	3	3	1 Be, 2 M
Lk Hα 234	8.5	1.00	1.1	20	7	5	1 Be, 1 B, 2 K, 1 Me
RR Tau	8.4	0.80	0.5	5	5	0	–
VV Ser	7.5	0.44	1.0	30	25	15	1 Be and mostly K stars
BD +46° 3471	7.3	0.90	1.0	11	9	9	1 Ae, 1 G, 3 K, 2 M, 2 Me
HD 200775	7.2	0.60	1.0	7	4	4	1 Be, 1 Fe, 1 Ke, 1 Me
BD +61° 154	5.1	0.65	1.0	12	10	5	1 Be, 4 K
Lk Hα 208	4.1	1.00	0.7	6	3	0	–
HD 250550	3.9	0.70	0.7	7	5	2	1 Be, 1 early K
Lk Hα 218	3.8	1.15	0.5	5	3	0	–
Lk Hα 233	2.6	0.88	>0.6	2	2	2	1 Ae, 1 Me

Column (2): Stellar mass repeated from Table 1.1.
Column (3): Relative source distance normalized to 1 kpc.
Column (4): Relative instrumental sensitivity computed from $\sqrt{(exposure\ time/144\ s)} \times (telescope\ diameter/2.4m)$; HD 259431 and Lk H$\alpha$ 233 are given as lower limits due to relatively lower throughput infrared images.
Column (5): Number of K-band sources detected over 1/3 pc × 1/3 pc area; estimated error is $\sqrt{N}$.
Column (6): Number of detected infrared sources in (5) with optical counterparts.
Column (7): Number of optical counterparts in (6) with classification spectra.
Column (8): Comment on spectral types of cluster members, where available.

would be minor, and thus our ignorance of them does not significantly affect our discussion of stellar surface densities below.

We assess the relative sensitivity of our infrared images to various stellar populations based on comparison to the BD +40° 4124 region, shown in Figure 5.1. There are two types of effects which we consider: those due to instrumental parameters and those due to source parameters The total measure of relative sensitivity is given by $\sqrt{t_{exposure}} \times diameter/distance$, where $t_{exposure}$ is the total integration time per pixel normalized to 144 seconds, *diameter* is the telescope diameter normalized to a 2.4m telescope, and *distance* is the source distance normalized to 1000 pc. Our choice for the normalization distance is based on the physical completeness limits presented in Table 3.2. For this combination of integration time, telescope size, and distance, our survey is sensitive at K to all masses down to 0.1 $M_{\odot}$ as long as the source is obscured by less than 10 visual magnitudes and has an age less than 1 Myr.

Each of the two pieces of the sensitivity correction are listed in Table 5.1. Were these numbers to be interpreted as correction factors, the mean instrumental correction factor (including only integration time and telescope area) is about 20%, while when distance corrections are included the mean correction factor is about 10%. Additional consideration for total system throughput might also be made, but rigorous throughput numbers are quite uncertain due to changes in thermal background and/or sky conditions with time; cases where the system throughput is expected to be significantly lower than the average (*e. g.* for the SQIID frames) are noted as lower limits.

Figure 5.3 shows a histogram of the relative sensitivity of our infrared images. As can be seen from this Figure, our sensitivity limits are the same in all regions to within a factor of two, normalized to the BD +40° 4124 region. From $m_1 - m_2 = -2.5\ log(f_1/f_2)$, a factor of two in sensitivity translates into a range of

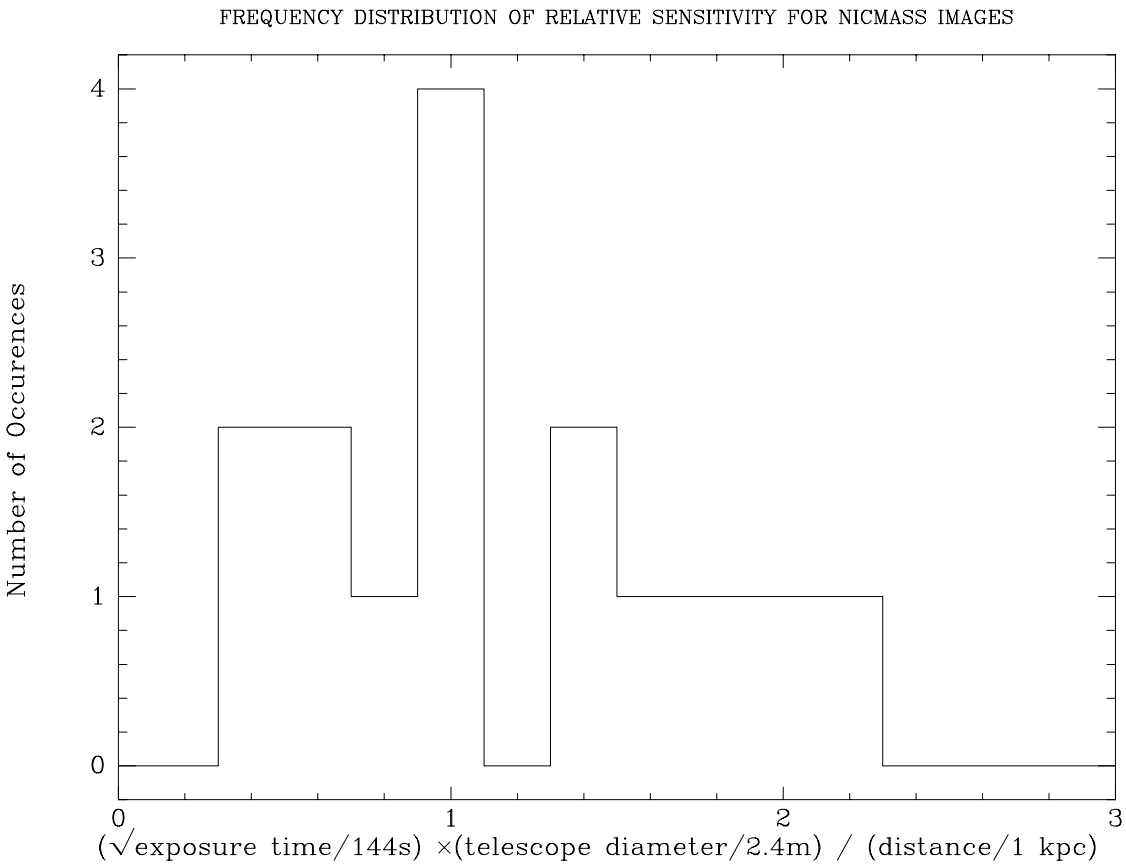

Figure 5.3. *Histogram of relative infrared sensitivity between Ae/Be regions in this survey.* Relative sensitivity between our infrared frames can be computed as $\sqrt{t_{exposure}} \times diameter/distance$, which we normalize to 144 seconds of total integration time on a 2.4m telescope for a source at 1000 pc with the NICMASS camera. We calculate this quantity in order to assess the relative depth of our data in each Ae/Be region. To first order, our sensitivity limits appear to be the same in all regions to within a factor of two.

about 0.8 magnitudes. We can use this information to compare our K-band survey limits to model K-band magnitude functions, calculated for clusters with masses distributed according to a Miller-Scalo mass function and ages appropriate for pre-main sequence populations. By comparing to the models (*cf.* those by Ali & DePoy 1994), we find for clusters of age 10 Myr or less, that our survey falls on the flat or *falling* part of the predicted K-band magnitude distribution. Thus a range of 0.8 magnitudes in survey sensitivity corresponds in the worst case (a 10 Myr old cluster) to only a 25% correction to our true source counts; the implied corrections are significantly smaller for younger clusters. We thus estimate the source count corrections from the K-band sensitivity differences between Ae/Be regions to be $< 10\%$. We do not attempt such small corrections.

Henceforth ignoring sensitivity differences, we in Figure 5.2 show a histogram of the number of infrared sources detected on the images in Figure 5.4. The mean number of companions found within 0.167 pc of high-mass Ae/Be stars is about 10. We note that when the variations in sensitivity between different regions *are* considered, the BD +40° 4124 frame ($M_{Ae/Be} = 13\ \mathrm{M}_{\odot}$) and the HD 250550 frame ($M_{Ae/Be} = 4\ \mathrm{M}_{\odot}$) are found to have the same physical limits in mass, age, and extinction. However, as can been seen from Figure 5.2, these two stars have very different local clustering characteristics. We simply note this fact now, but return to it in a forthcoming argument (section 5.3.3) for a trend of stellar density with Ae/Be mass over 0.167 pc radial size scales.

In summary, we have presented source counts derived from our infrared imaging survey and assessed in a quantitative manner the applicable corrections to the census numbers differences in our data in instrumental sensitivity and source distance. We find the corrections to be small and disregard them. Before moving to our discussion of stellar densities, however, we would like to examine our survey parameters and the possibilities that our census counts may include as associated

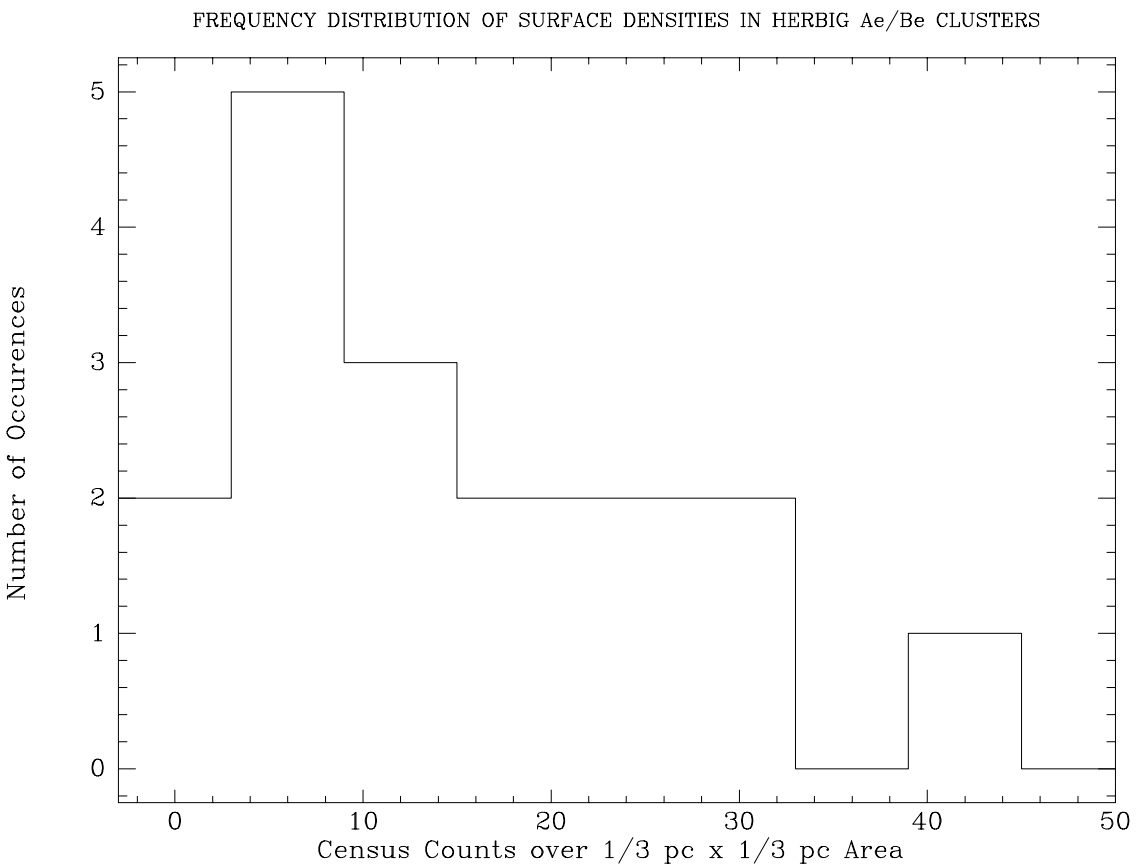

Figure 5.4. *Histogram of census counts within 0.167 pc of Ae/Be stars.* While the actual number of infrared companions over an area of linear size 1/3pc per side is uncertain due to correction factors (see text), this figure estimates the range of cluster sizes / densities between Ae/Be regions.

group members, either too few (hidden from our survey) stars too many (physically unassociated) stars.

5.2.1 Survey Completeness

First we address completeness issues related to our survey sensitivity limits (in mass, age, and extinction).

For the purpose of assessing our survey sensitivity to various stellar populations, we will anticipate the results of our analysis of HR diagrams and infrared color-magnitude diagrams in Chapters 8 and 7. From the location of optically visible stars in HR diagrams, we find that the stellar populations associated with young Ae/Be stars are also young ($\tau < 3$ Myr). In the infrared, where we are more sensitive to older, less massive, (*e. g.* less luminous) stars than we are in the optical (see Tables 3.1 and 3.2), the distribution of sources in $J-(J-H)$ color-magnitude diagrams instead shows all points detected to lie above a lower envelope defined by the reddening vector projected from the 0.1 $M_{\odot}$ point on the 3 Myr isochrone. To our completeness limits in A_V (which are always important to keep in mind), we find no evidence for stellar populations older than 3 Myr; the mean ages are more typically 1 Myr or less. This information suggests that we could be missing low-mass stars from our infrared surveys only if they are older *and* more heavily extincted than the rest of the stellar population. (If the low-mass stars were slower in clearing away obscuring circumstellar material than their higher mass counterparts, this scenario could apply.) We are unlikely to be missing low-mass stars if their ages are comparable to those derived for the surface populations, and thus we are confident that at the typical distances of our sources, our deepest infrared frames have captured most of the populations associated with the Ae/Be cores.

Regarding extinction, due to the unknown size scale of spatial variations in cloud column density, combined with the inherently large telescope beam sizes, we have not attempted to account for differences in mean column density between regions. We note, however, that the range of mean core extinction values runs from A_V = 2-20 mag, which corresponds to a range in extinction at 2.2 μmrunning only from A_K = 0.2-2 mag. We thus disregard differences in molecular extinction between Ae/Be cores.

A proper assessment of completeness in imaging surveys of star-forming regions requires rigorous region-by-region analysis of both instrumental sensitivity and mean molecular column density. To make completely fair comparisons between regions, stellar populations studies should be performed down to uniform limits in mass, age, and extinction. However, given 1) the absence of precision information on stellar masses, ages, and extinction values, and 2) the small number statistics with which we begin, we are content to have convinced ourselves that we are not dominated by incompleteness effects. We conclude, based on the apparent extreme youth of the Ae/Be stars and their surrounding stellar populations relative to our survey sensitivity limits, that the 1/3 pc $\times$ 1/3 pc fields over which we investigate each Ae/Be site allow us to capture a significant fraction of any accompanying stellar population, with the following characteristics: $M > 0.12$ $M_\odot$, $\tau < 1$ Myr, and $A_V < 10$.

5.2.2 Survey Contamination

Next we address whether our fields might be affected by severe foreground or background contamination from cluster nonmembers projected onto the cloud cores.

One means of probing the number of interloping foreground and background stars is with analytic models of the Galactic stellar distribution. Jarrett (1992)

describes an implementation of the Bahcall-Soneira model in which monte-carlo methods are used to calculate the expected properties of stars seen towards a given direction of the Galaxy over a given solid angle. With this method we can, in principle, obtain estimates of the spectral types, distances, and apparent magnitudes and colors for sources expected to populate a particular field. However, the applicability of the Bahcall-Soneira model, which reproduces the optical sky at high Galactic latitudes remarkably well, in the infrared ($\lambda > 1$ μm) and near the Galactic plane ($b < 5°$) is uncertain at the present time. A more realistic Galaxy model proposed by Ortiz & Lepine (1993; see references therein for others) includes the non-negligible effects of spiral structure, interstellar extinction, and the intrinsic colors of special stellar populations such as AGB stars. As these authors demonstrate, their model reproduces equally well at V and significantly more accurately at K (to within 0.2 dex for K $<$ 10 mag), the observed source counts in several well-separated directions of the Galaxy, when compared to the Bahcall-Soneira model. However, the observational data to effect accurate comparions between different models for fainter stars, such as those which dominate our surveys, are not yet available. Due to the severe uncertainties in the accuracy of available Galaxy models 1) at near-infrared wavelengths and 2) at low Galactic latitudes, we thus reject an analytical treatment of foreground / background issues in favor of an observational assessment of the degree to which our cluster samples might be contaminated. In the following we review our empirical investigation of contamination by nonmember stars.

Foreground stars can be identified on the basis of low extinction values in comparison to the canonically expected extinction of 0.9 mag / kpc in the Galactic plane. We will discuss the determination of extinction towards individual stellar sources in Chapter 8. If we can anticipate and generalize our results from the few regions rigorously analyzed to date, however, we suspect foreground contamination

to be acceptably low (0-1 star) over fields a few arcmin^2 in size, for sources at distances of less than 1 kpc and at latitudes within 3 degrees of the Galactic plane. We base this claim on the following: Given the completeness limits of our combined optical / infrared surveys, any foreground star detected in the infrared frames should also be detected in the optical frames. Amongst optically visible sources, 80-100% show both spectroscopic emission lines and near-infrared excesses, indicating that at least this many stars are cluster members and not foreground stars. The fractional contamination due to foreground stars for any individual region of course varies significantly with distance and proximity to the plane. Of note, however, is that we see no correlation between the number of detected companions and the source distance, as might be expected if foreground contamination were severe.

Background stars (we are most susceptible to contamination by distant, luminous background K,M giants and slightly background F,G dwarfs) can be identified on the basis of high extinction values in comparison to the maximum extinction through the core derived from LTE analysis of molecular data. There are two complications to this seemingly straightforward exercise, however. First, one might imagine the LTE analysis to produce only lower limits to the total core extinction, given the large beam sizes and the high likelihood of molecular photodissociation over radii of at least several tenths of a pc near young early-type stars. Second, the molecular core medium is likely to be clumpy, with young embedded sources possibly suffering additional circumstellar extinction. Thus pockets of locally high obscuration are not unlikely, and make young heavily embedded cluster members indistinguishable from distant cluster nonmembers in the absence of other youthful diagnostics such as continuum infrared excess or spectroscopic emission. Given the peculiar cloud structures identified in our molecular survey and the unknown degree of cloud clumpiness, we are reluctant to

identify any particular sources amongst our small cluster populations as background on the basis of high extinction. Based on infrared color-magnitude diagrams, however, it is clear that we are not dominated by background contamination as we do not see *any* stars lying below the main sequence loci. We also note that the stellar clusters associated with Ae/Be stars do not appear to be superposed on uniformly distributed backgrounds of infrared sources. Instead, the aggregates are in many cases concentrated towards the centers of our several arcmin images, with only a small number sources located in the outer portions of the images. We conclude that core extinction effectively shields background stars from our detection. Of note is that we see no (anti-)correlation between the number of detected companions and the mean molecular extinction.

In summary, we have bypassed a quantitative treatment of foreground / background contamination, given the uncertainties derived from comparison of Galactic model star count predictions as a function of magnitude (down to $K \approx 15$) with those actually seen in our own photometric / spectroscopic surveys in regions near the Galactic plane. In general, the number of foreground stars seems overpredicted by the models and we thus have reduced confidence in the background predictions. Instead, we have qualitatively argued that fractional contamination from sources at distances different from those of the Ae/Be stars themselves, is likely to be low ($\lesssim 10\%$) over the inner 0.167 pc radii of the Ae/Be clusters. Therefore, instead of attempting uncertain foreground / background corrections, we assume all sources in our surveys to be cluster members and proceed with our analysis of the cluster properties.

5.3 Projected Stellar Densities in the Vicinity of Ae/Be Stars

5.3.1 Comparison with Other Regions of Star Formation

Although we have already stated that absolute number densities are difficult to derive with any confidence, for the purpose of making relative comparisons between regions, we use our census counts to compute the number of *stars* pc^{-3} assuming that the clusters are uniform and spherically symmetric. We find a range of volume densities from about 200-2000 pc^{-3} with a mean of about 1350 pc^{-3}. We compare the inferred number densities in the Ae/Be clusters to those in other star-forming regions, in the form of a number density line (shown in Figure 5.5) which depicts the densities characteristic of nearby low- and high-mass star-forming sites. (For reference, a number density of 1000 stars pc^{-3} translates into a mean separation of about 15,000 AU, including the $4/\pi$ correction factor for mean projection.) The cluster data are taken from McCaughren & Stauffer (1995) for the Trapezium region; Meyer *et al.* (1995) for NGC 2024, ρ Oph, and R CrA; Lada *et al.* (1991) for NGC 2023, 2068, and 2071 (these numbers may be underestimates due to the low sensitivity of these early observations); and Gomez *et al.* (1993) for Taurus, Lupus, & Chameleon T1. If the depth of our infrared survey is comparable to the completeness of the surveys in these other young, heavily extincted, nearby star-forming regions, we conclude from this Figure that the mean density for the Ae/Be clusters (indicated by a dagger) is higher by about a factor of 5 than the mean density for the nearby low-mass star-forming clouds, but lower by about a factor of 10 than that in the inner Trapezium region, perhaps an extreme example of a high-density star forming environment.

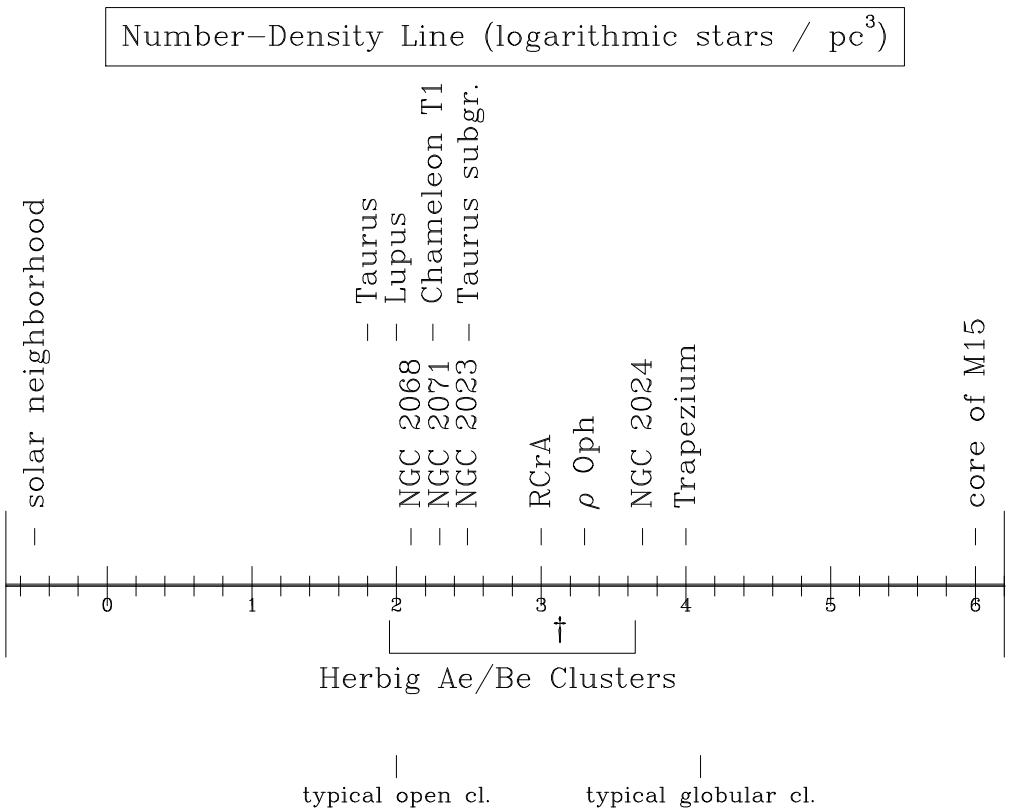

Figure 5.5. *General context of Ae/Be clusters densities.* The range of volume densities found to characterize the inner 0.167 pc of the Ae/Be clusters, and the weighted mean (dagger), are shown along a logarithmic line containing other well-studied star-forming regions. Typical open and globular cluster number densities are shown for comparison, as are the extrema of the solar neighborhood and the core of M15. We note that the star-forming regions containing intermediate- and high-mass stars have characteristically higher densities than those producing only lower-mass stars, but caution that computations of surface and volume densities always yield lower limits due to complications arising from extinction and/or cloud clumpiness.

5.3.2 Comparison with Other Isolated Massive Stars

How do the number densities in the young Ae/Be regions compare with those in equally isolated regions containing slightly older, early-type stars? Unfortunately the data necessary for a fair comparison do not exist as neither accurate stellar ages nor complete companion counts have been determined for any representative population of main sequence early-type stars. For isolated 5-10 Myr B stars, the data on companions which do exist are in the form of infrared surveys, Hα surveys, and x-ray surveys.

From near-infrared survey data we can discuss the S 255/S 257 and MonR2 regions. In the S 255/S 257 region, two main sequence B0 stars with assumed ages of several Myr are found on either side of an extremely young embedded stellar cluster; however, there appear to be *no* young stars located within several tenths of a pc of the B stars themselves (Zinnecker, McCaughren, & Wilking; 1993). We find the same situation in the MonR2 region where, again, there are two main sequence B stars of ages 6-10 Myr on opposite sides of an embedded young dense cluster with very few companions (within 0.167 pc there is 1 in the case of the eastern star and several in the case of the western star) of their own (Dougados *et al.* ; 1995). From Hα survey data we can discuss the σ Sco and ν Sco regions. Sigma Sco is a B1 III with a well determined age of 5-6 Myr; the region within 1.3 pc has been completely surveyed in the far-infrared and at Hα with only 8 young low-mass companions (corresponding to 1 within a 0.167 pc radius) uncovered (Meyer, Wilking, & Zinnecker; 1992). The results in Nu Sco appear similar, as only 13 young companions over an even larger area were reported in the Hα survey of Thé (1964). From x-ray survey data we can discuss the β Sco and δ Sco regions. Both of these 5-6 Myr old B stars have had x-ray exposures centered on them (Walter; 1994) which reveal in each case only 5 companions within 1.4 pc (corresponding to less than 1 within a 0.167 pc radius).

Summarizing the information available from infrared, Hα , and x-ray surveys in the vicinity of isolated, slightly older ($\tau > 5$ Myr) early-type stars without evidence for remnant molecular gas, it seems to be the case that very few nearby young lower-mass companions to these stars can be found. We contrast this trend with that presented above on dense clusters associated with the significantly younger ($\tau < 1$ Myr) population of Ae/Be stars (which *are* still associated with molecular gas). It could be the case that the scant evidence on which we base the lack of companions to older early type stars simply reflects that these surveys are not sensitive to highly reddened low-mass stars with ages of several Myr. On the other hand, this information is also consistent with the interpretation that if all high-mass stars are formed within the boundaries of small, dense clusters of stars, that the timescale for cluster dispersal is comparable to the timescale for the "evaporation" of molecular gas.

5.3.3 Correlation of Cluster Density with Maximum Stellar Mass

The images presented in Figure 5.2 are organized in order of decreasing Ae/Be mass. Disregarding the slight differences between regions in survey sensitivity (discussed above), these images provide the impression that there is some relationship between the number of companions and the mass of the central Ae/Be star. The range of stellar masses represented in the first page of images in Figure 5.2 is roughly $10 - 25$ $M_{\odot}$, and the mean number of stars detected is 23. The range of stellar masses represented in the last page of images in Figure 5.2 is roughly $3 - 5$ $M_{\odot}$, and the mean number of stars detected is 6. Larger stellar densities in regions producing higher mass stars might be expected if the presence of a cluster were important, during the initial formation processes, in determining the final masses of high mass stars (see discussion in the following section). We

can investigate the observational support for such a possibility by correlating the number density of infrared companions with the mass of the central Ae/Be star.

Stellar densities, in units of $stars\ pc^{-3}$, are directly proportional to the census numbers we have presented in Figure 5.4, but are uncertain by correction factors due to cluster projection and concentration effects, both of which can be as high as 30%. Thus, in Figure 5.6, we instead show stellar surface densities, computed simply as the number of stars detected in an area 1/3 pc on a side, as a function of Ae/Be mass. For reference, we also show the same computation for the Trapezium Cluster. Although the scatter is large (significantly larger than the error bars, which are presented as random errors of 10% in the stellar masses and $\sqrt{N}$ in the cluster census counts), the apparent trend is very suggestive of a physical relationship between cluster density and maximum mass at very young ages. A least squares fit to this log-log distribution, including errors in the independent quantities, reveals a linear relationship of near unity slope and correlation coefficient 0.8.

Before interpreting this diagram, we would like to investigate two possible systematic effects with Ae/Be mass which might affect the origin of the apparent correlation: differences between regions in actual cluster/cloud size, and differences between regions in total core extinction.

First, how are our results affected by the assumption of a *constant cluster size*, corresponding to a radius of $\frac{1}{2}\times$ 0.33 pc = 0.167 pc? To properly determine actual cluster sizes, one would like to know the FWHM of the two-dimensional stellar density distribution and then count stars over this physically meaningful area; however, given the small number statistics within the r=0.167 pc regions with which we begin, division of the clusters into several radial bins is not meaningful. We have, however, used the BD +40° 4124 group, in which isolated clustering has been clearly demonstrated (see Figure 5.1), to identify the scale over which we

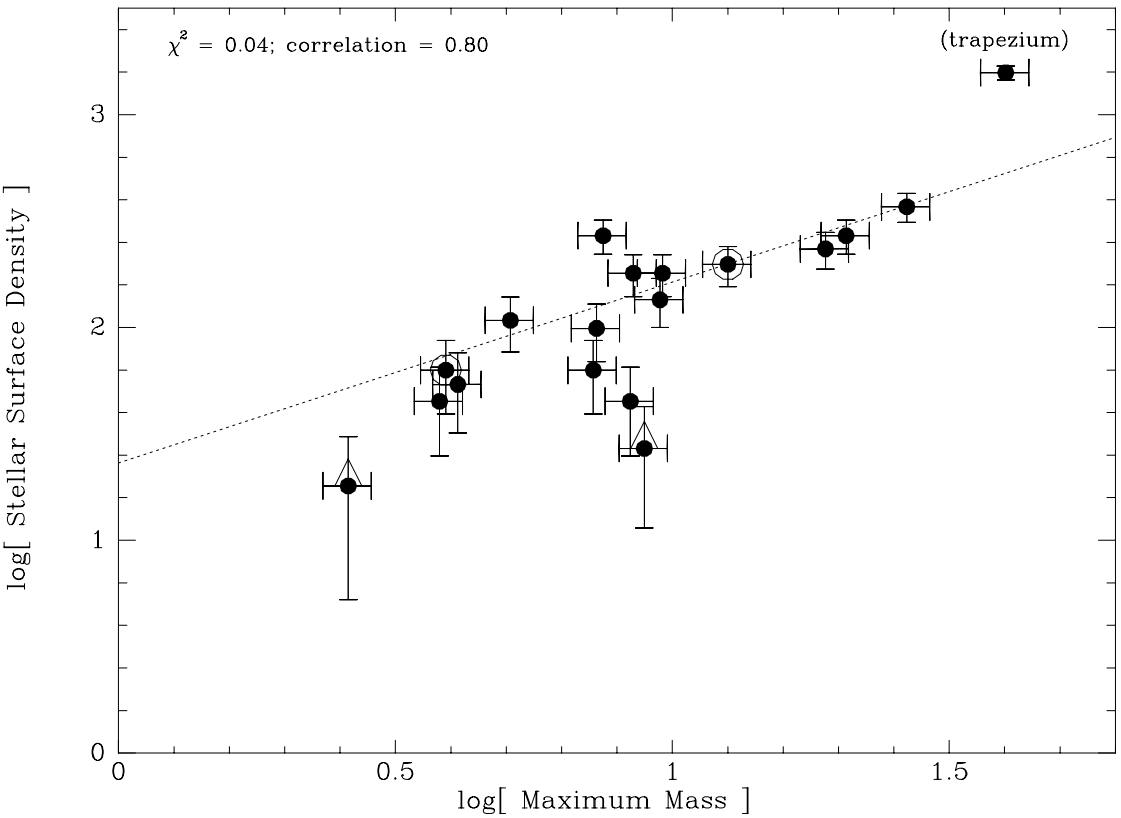

Figure 5.6. *Stellar surface density versus maximum mass for clusters associated with Ae/Be stars.* A quantity proportional to the stellar number density is plotted against the mass of the most massive star in the group. Larger open circles indicate groups in which the relative sensitivity factor described in the text is unity. Triangles represent lower limits in two cases where the images are significantly less sensitive. Random errors of 10% in the stellar masses and $\sqrt{N}$ in the cluster census counts are shown. We note that the regions containing more than one Ae/Be star do not occupy any preferred location in this diagram. The inner 0.167 pc of the Trapezium Cluster, for which the stellar density was computed in the same manner as for the Ae/Be regions, is also shown, for reference only. A line which accounts for the errors in both axes has been fit to the data distribution (not including the Trapezium or the lower limits) and produces a correlation coefficient of 0.8.

investigate the clustering properties for all groups in our sample. Based on the cloud radii derived from our molecular survey (given as $1/2 \times FWHM(A_V)$ in Table 2.1, and apparently independent of Ae/Be mass), this radius enables us to count stars over the inner 35-100% of every cloud core. There is, however, qualitative evidence in Figure 5.2 for concentration of sources towards a few of the central Ae/Be stars, particularly in the cases of MWC 1080, MWC 137, and BD +40° 4124. Quantifying this impression though, would require either nearest-neighbor analysis or two-point correlation analysis over regions of larger size than we have considered here. Alternate to actual concentration, the data are also consistent with the clusters associated with these sources simply being smaller than in the typical case. In other words, if $r_{cluster} \leq 0.167\ pc$, we are unable with our method of computing surface densities, to distinguish between

$$N_{total} = \int_0^{r_{cluster}} 4\pi r^2 n(r) dr$$

and

$$N_{counted} = \int_0^{0.167\ pc} 4\pi r^2 n(r) dr.$$

Although in this case we are assured of including all cluster members in our census counts, we systematically underestimate the stellar densities. If, on the other hand, $r_{cluster} > 0.167\ pc$, as is likely in most cases given the apparent sizes of the cloud cores, then in princple we should be sensitive to concentration on smaller scales. In this case we systematically underestimate the total number of associated stars but do determine accurate stellar densities. In summary, while it seems that the cluster densities do depend critically on the chosen cluster radius, we find no effects as a function of Ae/Be mass by assuming a constant cluster radius between regions. We note, however, that a more appropriate analysis of Ae/Be clustering properties might include the calculation of rank-ordered nearest neighbors.

Second, might the trend of stellar density with maximum mass be artificially produced due differences in *mean cloud core extinction*, which varies by up to a

factor of 10 between Ae/Be regions? One might posit that differences in core extinction could permit us to see larger numbers of companions around higher mass stars, for example, if the higher-mass stars are more efficient in clearing away core material. We have investigated this possibility by plotting maximum mass versus molecular column density and stellar number density versus molecular column density; we find no correlations.

With no evidence for systematic effects due either to intrinsic cluster size variations or to core extinction variations, we conclude that the trend of stellar density with maximum mass represents a real relationship between these two independent quantities over more than an order of magnitude. Can we relate this trend to theoretical predictions on hierarchical fragmentation / clustering in molecular cloud cores? We address this issue in the following section.

5.3.4 One Interpretation of the Correlation

If our apparent finding that local stellar density correlates with maximum stellar mass holds as a robust result, it could represent an important clue to the formation processes associated with intermediate- and high-mass stars. In particular, higher mass stars might be expected to be found near the centers of dense clusters if, during the initial accretion stages, cluster dynamical effects which enhance accretional growth are important. In this section we first review the theoretical difficulties with producing high-mass stars in a manner analogous to that in which low-mass stars are thought to form. We then comment on previous speculation in the literature that the mass of the most massive star in a group might be related to protostellar dynamical evolution, and/or the critical mass for core fragmentation.

Current star formation theory accepts the notion of a preferred length scale which separates the domain of domination by thermal pressure against gravity

from that of domination by turbulent or magnetic pressure against gravity, in molecular cloud cores. The critical thermal length scale, given by

$$\lambda = \sqrt{\frac{\pi c_s^2}{G\rho}} \leq c_s \tau_{ff}$$

(in which c_s is the local sound speed, ρ is the local density, and τ_{ff} is the local free-fall timescale), represents the size of the smallest clump which is able to overcome hydrostatic support and collapse to form a star. The characteristic mass associated with the thermal length is the Jeans mass,

$$M_J = \frac{4\pi}{3}\rho(\frac{\lambda}{2})^3$$

or, substituting for λ (above) and $c_s = \sqrt{P/\rho} = \sqrt{kT/\mu}$,

$$M_J = (\frac{T}{10K})^{3/2}(\frac{\rho}{5 \times 10^{-19} g\ cm^{-3}})^{-1/2} \quad \mathrm{M}_\odot.$$

For a typical range of cloud core conditions, the Jeans length ranges from about 0.05-0.3 pc and the Jeans mass ranges from about $0.5 - 2$ $\mathrm{M}_\odot$.

A well-known inconsistency in Jeans collapse theory is the following: as collapse proceeds, the mean density necessarily increases and, as the opacity subsequently rises, the mean temperature also increases. However, before equilibrium can be restablished, the Jeans length/mass has effectively grown smaller; initally Jeans-unstable cores are thus able to fragment and sub-fragment in what is most likely a hierarchical process. [1] Even rigorous analyses (including the effects of rotation and magnetic fields; Larson, 1985) of hydrostatic stability in the more realistic case of pressure-supported sheets or thin filaments instead of in the classic case of uniform-density spheres, yield characteristic length and mass

[1] The results of Gomez *et al.* (1993) and Larson (1995) suggest that the observed separations of young stars in Taurus and Ophiucus can be represented by two power-law indices for separations spanning 3 orders of magnitude, from 0.005 - 5 pc. A break in the power-law index at 0.04 pc (approximately the Jeans length for these low density clouds) is claimed by Larson (1995) to distinguish the hierarchical clustering regime from the binary regime.

scales for fragmentation. Strong observational support for fragmentation comes from the common finding of several tens of stars which have formed within a single Jeans length, as we have seen here.

A second problem with Jeans collapse theory is that the characteristic mass is *inversely* related to the mean density, implying that low-mass stars should form in dense cores while high-mass stars should form only in low-density cores. This is inconsistent with the prevalent association of dense gas with high-mass star-forming regions, including many of the Ae/Be cores studied here, and suggests that "special conditions" may be required for high-mass star formation. One possibility is the continuing accretion of material at late times in dense proto-stellar environments, a process which could be aided by the settling of the most massive objects towards the center of the system due to dynamical friction (Larson, 1978, 1981, 1992; Bastien, 1981).

Based on the observations presented here on clusters associated with young high-mass stars, we find ourselves facing the difficult problem of having to produce in the same cloud cores *both* clusters (presumably via fragmentation) *and* high-mass stars (presumably via accumulation in an environment where the accretion of ambient core material is a competitive process between many proto-stellar cluster members). Thus hierchical fragmentation and hierarchical clustering / accretion appear to be operating simultaneously. The trend of stellar density with maximum mass could be a fundamental clue to how these processes might work. As Larson (1991, 1992) speculates, it may be that mass of the most massive star formed in a cluster depends on some combination of the two fundamental scales discussed above: 1) the Jeans mass and 2) the total cluster mass.

5.4 Conclusions and Discussion on Ae/Be Clustering Properties

We have discovered small aggregates of apparently low-mass stars located in the same molecular cores as are high-mass Ae/Be stars. It is not unusual to have identified clusters of low-mass stars associated with high-mass stars, as it is known that the same molecular cores are capable of producing stars of all masses. However, what is new about this study is the age range ($\tau < 1$ Myr), the mass range ($M > 3$ M$_\odot$), and the size scale ($r < 0.167$ pc), of the high-mass star-forming environments we have targeted for investigation. The uncovered stellar populations can be described as containing between 5 and 40 stars and, under the assumption of spherical symmetry, as having stellar volume densities over radii of 0.167 pc ranging between 200 and 2000 pc^{-3}. The apparent youth of the clusters (which we confirm in subsequent Chapters) suggests that the stars are near their places of birth, and thus that we are observing "initial" cluster conditions. These regions seem amenable, therefore, to investigation of issues related to the "initial" distribution of stellar masses, which we pursue in Chapter 9.

Regarding stellar masses, we draw attention to the BD +40° 4124, Lk Hα 198, and Lk Hα 234 regions as examples of molecular cores in which two (or more in the case of BD +40° 4124!) intermediate-mass ($M > 1$ M$_\odot$) stars have formed within 0.1 pc of one another. These groups are rare in that, assuming a typical cluster size of about 10 stars (Figure 5.4), only 1 out of every 10 random groups of 10 stars is expected to contain a single star of mass $M > 5$ M$_\odot$ (according to the tabulations of Miller & Scalo (1979)), and so only 1 out of every 100 random groups of 10 stars is expected to contain *two* stars of mass $M > 5$ M$_\odot$. The local regions producing more than one Ae/Be star seem worthy, therefore, of detailed investigation in order to determine whether they are biased in some manner towards producing intermediate- and high-mass stars. We return to these thoughts in later discussion.

We have found an apparent trend of stellar density with the mass of the central Ae/Be star, which may find explanation in the local clustering and environmental conditions necessary to produce high-mass stars. We further address these issues in our discussion (Chapter 10).

Finally, our imaging data provides the basis for identifying stars located within several arcsec of the Ae/Be stars. This information can be used to address issues related to binaries and to the spectral energy distributions of the Ae/Be stars themselves. First, translated into physical units, the (projected) separation range to which we are sensitive to binary companions is several hundred to several thousand AU (depending on source distance), although of course no dynamical evidence exists that these stars are actual binaries. Second, the brightness of nearby infrared companions is important for understanding the potential contribution of red, low-mass stars to the inferred infrared excesses for the Ae/Be stars. We present our assessment of the data relevant to the binary and the spectral energy distribution issues in Appendix B.

5.5 Plan for Remainder of Presentation

Having established that small clusters are typically found in nearby association with Ae/Be stars, our discussion henceforth will focus on the properties of the individual stars comprising the clusters. In particular, we will examine four groups – those assicated with BD +40° 4124, Lk Hα 215, MWC 1080, and Lk Hα 234. Our goals are to establish the ages and masses of individual cluster members, and the age spreads and mass spectra of the stellar groups. We first verify our previous assertion that most of the members of the inner Ae/Be aggregates have the optical spectrocopic and infrared photometric signatures of accreting low-mass pre-main sequence stars (Chapter 6). We then discuss infrared color-magnitude diagrams (Chapter 7), which enable us to make a first-order characterization of the stellar

populations comprising the Ae/Be clusters. We then place the optically visible members of the aggregates in a theoretical HR diagram (Chapter 8) from which we can determine their relative ages and masses. Finally we present our statistical technique for investigating the distribution of stellar masses in clusters with small numbers of members (Chapter 9).